J. Ocean Univ. China (Oceanic and Coastal Sea Research)
https://doi.org/10.1007/s11802-018-3676-6
ISSN 1672-5182, 2018 17 (5): 1091-1102
http://www.ouc.edu.cn/xbywb/
E-mail:xbywb@ouc.edu.cn

Estimation of S-wave Velocity for Gas Hydrate Reservoir in the Shenhu Area, North South China Sea

LIU Xueqin[1), 2)], XING Lei[1), 2), *], and LIU Huaishan[1), 2)]

1) *Key Laboratory of Submarine Geosciences and Prospecting Techniques*, *MOE and College of Marine Geosciences*, *Ocean University of China*, *Qingdao* 266100, *China*
2) *Evaluation and Detection Technology Laboratory of Marine Mineral Resources*, *Qingdao National Laboratory for Marine Science and Technology*, *Qingdao* 266071, *China*

(Received September 19, 2017; revised January 18, 2018; accepted March 4, 2018)

Abstract Estimation of S-wave velocity using logging data has mainly been performed for sandstone, mudstone and oil and gas strata, while its application to hydrate reservoirs has been largely overlooked. In this paper we present petrophysical methods to estimate the S-wave velocity of hydrate reservoirs with the P-wave velocity and the density as constraints. The three models used in this paper are an equivalent model (MBGL), a three-phase model (TPBE), and a thermo-elasticity model (TEM). The MBGL model can effectively describe the internal relationship among the components of the rock, and the estimated P-wave velocities are in good agreement with the measured data (2.8% error). However, in the TPBE model, the solid, liquid and gas phases are considered to be independent of each other, and the estimation results are relatively low (46.6% error). The TEM model is based on the sensitivity of the gas hydrate to temperature and pressure, and the accuracy of the estimation results is also high (3.6% error). Before the estimation, the occurrence patterns of hydrates in the Shenhu area were examined, and occurrence state one (the hydrate is in solid form in the reservoir) was selected for analysis. By using the known P-wave velocity and density as constraints, a reasonable S-wave velocity value (ranging from 400 to 1100 $m\,s^{-1}$ and for a hydrate layer of 1100 $m\,s^{-1}$) can be obtained through multiple iterations. These methods and results provide new data and technical support for further research on hydrates and other geological features in the Shenhu area.

Key words S-wave velocity estimation; hydrate reservoir; rock physical model

1 Introduction

Measurements of S-wave velocity have played a very important role in the recent development of seismic exploration. Multiple methods of S-wave velocity estimation have been proposed. For example, Milholm *et al*. (1980) and Castagna *et al*. (1985, 1993) performed a series of rock physical experiments from which empirical equations were derived to estimate the P-wave velocities of limestone, sandstone, and shale. Li (1992) also presented a new nonlinear formula for quantifying the relationship between the P-wave and S-wave velocities. Xu and White (1995) proposed the Xu-White model based on their theories on sand and shale, and Nur *et al*. (2000) proposed the concept of a critical porosity model. Krief *et al*. (1990) presented a model for predicting the S-wave velocity that was very similar to the critical porosity model, but it extended the Gassmann empirical equation to other pore-fluid types. Zhang *et al*. (2013) modified the Xu-White model and obtained good results in estimating the S-wave velocity in carbonate formations. Dong *et al*. (2014) established a new shale rock physical model combined with the Brown-Korringa solid replacement method. By combining 3-D high-resolution seismic data and seabed high-frequency seismometer (OBS) data, Zhang *et al*. (2014) obtained P-wave velocities using seismic reflection profiles and the coherent inversion of multi-wave information. Furthermore, Lin (2015) proposed a model to predict the S-wave velocity in sand-shale formations using multi-well statistics and rock physical modeling. Cheng *et al*. (2018) imaged P-and S-wave velocity structures in hydrate bearing sediments along an OBS profile across the Yuan-An Ridge, off southwest Taiwan. Xing *et al*. (2018) studied the sensitivity of P-waves and S-waves to gas hydrate in the Shenhu area using OBS. Estimations of S-wave velocity on logging data have mainly been performed for sandstone, mudstone, carbonate and limestone. However, there is little research on the S-wave velocity of hydrate reservoirs, especially based on the petrophysical model. The petrophysical parameters of elasticity are the key physical properties for studying hydrates. Therefore, it is the most direct and accurate method to

* Corresponding author. Tel: 0086-532-66782960
E-mail: xingleiouc@ouc.edu.cn

estimate the S-wave velocity of hydrate reservoirs by means of petrophysical model.

In this paper, we use three petrophysical methods to estimate the S-wave velocity in the Shenhu region, northern South China Sea. First, critical porosity theory is used to determine the porosity range of the Shenhu sea area. Then, the Gassmann saturated rock physical equation is used to determine the occurrence modes of the hydrates in the Shenhu area, and the solid and liquid phase models are compared. Then, using the P-wave velocity and the density as the constraint conditions, the S-wave velocity is estimated based on three different models. The reasonable S-wave velocity values (ranging from 400 to 1100 m s^{-1} and a hydrate layer of 1100 m s^{-1}) are obtained through multiple iterations. Due to economic and technical conditions, it is often difficult to measure S-wave data, and thus, it is significantly beneficial to accurately estimate S-wave data.

2 Logging Data and Petrophysical Parameters of the Shenhu Area

The Shenhu area, which is located on the northern slope of the South China Sea, is an important target area for marine gas hydrate exploration and development in China (Wu *et al*., 2007). Hydrate is not only a source of green economic energy but also has significant far-reaching impacts on global climate change, geological disasters (submarine landslides) and other activities that can destroy infrastructure, such as drilling platforms and submarine cables. Consequently, hydrates have been studied extensively in recent years (Ma *et al*., 2014; Wu *et al*., 2014). In 2007, the Guangzhou Ocean Geological Survey Bureau of the Ministry of Land and Resources of China organized and implemented the first oceanic hydrate drilling voyage (GHMS-1) in China. On this voyage, hydrate samples were successfully drilled in sites SH2, SH3 and SH7 (Fig.1).

Fig.2 records the five log curves obtained from SH2, from which it can be inferred no anomalous curves are found in the caliper curve. The thickness of the hydrate reservoir is approximately 30 m (spanning the depth of 190–220 m). The average velocity of the strata overlying the hydrate reservoir is approximately 1900 m s^{-1}, and the average velocity of the hydrate reservoir (190–220 m) is approximately 2070 m s^{-1}, with a maximum value of 2200 m s^{-1}. The average velocity of the strata underlying the hydrate reservoir is 1890 m s^{-1}. In the density curve, only the low-value region at 205–215 m corresponds to the acoustic velocity curve (representing the high-value region), and thus, in the hydrate mapping region the density curve is obviously less sensitive than acoustic curve. The resistivity curves are consistent with the acoustic curves, and high-value anomalies appear at depths of 190–220 m. The radioactive gamma curve does not record significant abnormalities in the hydrate storage area.

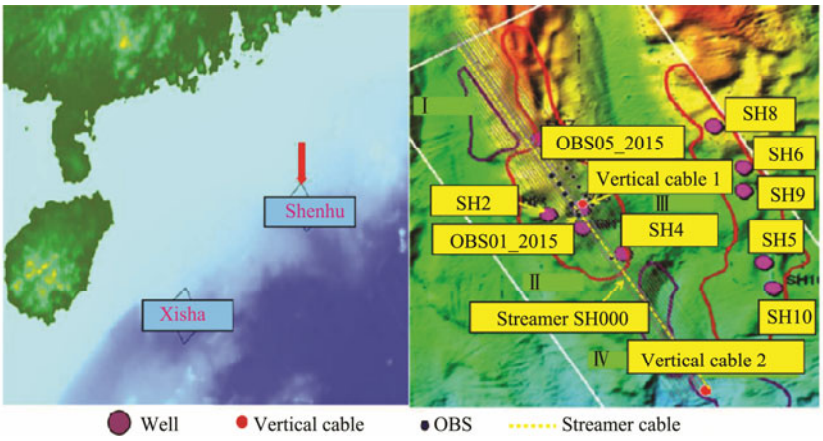

Fig.1 The South China Sea (left) and the Shenhu study area (right). In the right panel, the big red circle indicates the drilling location, and the well SH2 is near the location of the vertical cable. The symmetrical horizontal cable line represents the survey line (a total of 25 survey lines), and the yellow line marked in the middle of SH000 is the object line of this paper.

The porosity and the degree of hydrate saturation of the sedimentary layers hosting the hydrates (190–220 m) can be estimated from well log data using the density method and the Archie formula (Wang *et al*., 2011; Fig.2). The porosity of the hydrate-bearing layer increases from 40% to 50% but essentially remains above 40%. Therefore, this value represents the critical porosity of the solid-phase modulus of the rock (Ecker *et al*., 1998; Mavko *et al*., 2009). Thus, to estimate the S-wave velocity in this paper, the calculation method with the critical porosity greater than 40% must be selected. Additionally, the depth of the high saturation hydrate reservoir falls mainly between 195 and 210 m, in which the average saturation reaches 30% (Fig.2).

Table 1 provides the type and content of sediments in the Shenhu hydrate reservoir (Fu and Lu, 2010). The solid rock essentially consists of clay, sand and silt. In this paper, the physical parameters of sand and silt are assumed to be equivalent to those of quartz and calcite. The fluid phase is mainly composed of water and gas components. A variety of gas components can be present within hydrates, including hydrocarbon gases (such as methane and ethane) and compounds (such as hydrogen, carbon dioxide and hydrogen sulfide). However, the air analysis of

the sediments in the Shenhu area indicates that the main gas in the sediments of the Shenhu drilling area is hydrocarbon gas, with a maximum average methane content of 98% (Mavko *et al.*, 2009). Here, the average solid phase composition is used to estimate the initial iteration parameters. The fluid phase is estimated to contain 50% formation water and 50% gas initially, and the gas is assumed to be methane.

Table 1 Particle size composition of hydrate-bearing layers in the Shenhu area (using SH2 as an example) (Fu and Lu, 2010)

Drilling number	Particle size composition (%)				
	Layer	Clay	Silt	Sand	Quartz + Calcite
SH2	Upper layer	15.68–40.16	53.74–81.25	0.5–11.87	54.24–93.12
	Hydrate layer	20.46–30.33	72.02–77.09	0.75–2.68	72.77–79.77
	Lower layer	22.96–26.99	70.53–74.98	2.06–2.48	72.59–77.46

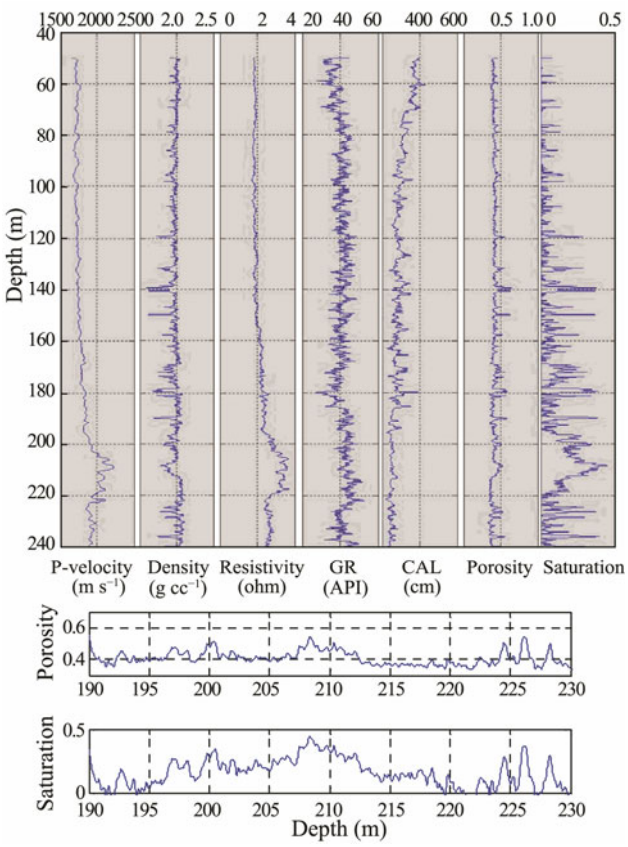

Fig.2 Curves of some parameters in original well SH2 and the partial enlarged view of porosity curve and saturation curve of the hydrate-bearing sedimentary layer.

3 S-Wave Velocity Estimation

Four types of occurrence models occur in the hydrate sedimentary layer, as shown in Fig.3. In the first and second types, the hydrate can become cemented in contact with rock particles or even wrapped around entire rock particles, thus becoming part of the rock skeleton and affecting not only the porosity of the rock but also the bulk modulus and shear modulus of the rock skeleton. The third type of hydrate forms at the grain boundary: in this cementing mode, the hydrate content directly affects the elastic modulus of the rock skeleton and significantly reduces the porosity of the rock.

Therefore, the first three cementation types are classified as the cementing model, in which the hydrate is a solid phase in the composition model. For the fourth type, hydrate is deposited in the matrix of the rock, potentially altering the bulk modulus of the rock pore fluid and becoming part of the rock fluid phase (Wang *et al.*, 2011). However, according to the concept of critical porosity (40%) (Mindlin, 1949; Nur *et al.*, 2000), researchers have classified it as the pore filling pattern when the porosity of the rock is less than the critical porosity (<40%), and the hydrate is treated as a fluid phase. But when the porosity of the rock is greater than the critical porosity (> 40%), the pore filling model is equivalent to the cementing model, and the hydrate is treated as a solid phase.

According to the IR-ray and X-ray scanning of hydrate samples obtained from the Shenhu area and the analysis of the sediment types and sedimentation patterns in the Shenhu area, it was confirmed that the hydrates were distributed in the pores of the clayey silt and silt (Chen *et al.*, 2009, 2011; Wu *et al.*, 2009; Wang *et al.*, 2011), but the porosity of the rock in the hydrate-bearing area is greater than the critical porosity (Fig.2). Therefore, in this paper, the pore filling model is used to study the hydrate, in which the hydrate participates among the rock skeletons as a solid phase of the rock.

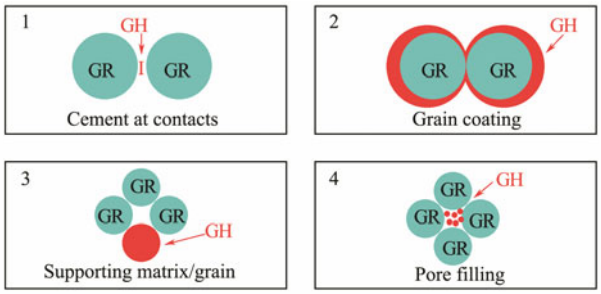

Fig.3 Micro-structural models depicting the gas hydrate layer (according to Dai *et al.*, 2004): 1) depicts the contact cementing type; 2) depicts the wrapping bond type; 3) depicts the cemented type; and 4) depicts the fluid cementing type.

3.1 Estimation of S-Wave Velocity Based on the MBGL Model

When the sedimentary layer does not contain hydrates, the elastic parameters of the dry rock can be calculated based on Hashin-Shtrikman-Hertz-Mindlin theory, and the saturated elastic modulus can be obtained from the Gass-

mann equation. According to the Hashin-Shtrikman-Hertz-Mindlin theory, there are two types of elastic moduli: one occurs when the rock porosity is greater than the critical porosity (ϕ_c=40%), in which the mineral particles are the carrier, and the other occurs when the rock porosity is less than the critical porosity, in which sediment particles are similar to suspensions relative to the major phase of the fluid phase.

When the porosity ϕ is less than the critical porosity:

$$K_{dry}=\left[\frac{\phi/\phi_c}{K_{HM}+\frac{4}{3}G_{HM}}+\frac{1-\phi/\phi_c}{K+\frac{4}{3}G_{HM}}\right]^{-1}-\frac{4}{3}G_{HM},$$

$$G_{dry}=\left[\frac{\phi/\phi_c}{G_{HM}+Z}+\frac{1-\phi/\phi_c}{G+Z}\right]^{-1}-Z,$$

$$Z=\frac{G_{HM}}{6}\left(\frac{9K_{HM}+8G_{HM}}{K_{HM}+2G_{HM}}\right). \quad (1)$$

The density of saturated rock is:

$$\rho=(1-\phi)\rho_S+\phi\rho_f, \quad (2)$$

where, ρ_S and ρ_f are the rock solid-phase and liquid-phase densities, respectively.

The effective modulus of elasticity at critical porosity is:

$$K_{HM}=\left[\frac{n^2(1-\phi_c)^2G^2}{19\pi^2(1-\sigma)^2}P\right]^{\frac{1}{3}},$$

$$G_{HM}=\left[\frac{5-4\sigma}{5(2-\sigma)}\frac{3n^2(1-\phi_c)^2G^2}{2\pi^2(1-\sigma)^2}P\right]^{\frac{1}{3}},$$

$$P=(1-\phi)(\rho_S-\rho_f)gh. \quad (3)$$

K_{dry} and G_{dry} represent the bulk modulus and the shear modulus of the rock skeleton, respectively. K_{HM} and G_{HM} represent the effective modulus of elasticity at the critical porosity. K and G are the bulk modulus and the shear modulus of the rock component (free of hydrates). σ is the Poisson's ratio of the rock component. P is the formation pressure; n is the number of the rock particles contacting with hydrates. Under normal circumstances, n=8.5. The elastic modulus of rock components is shown in Table 2.

Table 2 Elastic modulus of the main components of rock (using Quartz and Calcite instead of sand and silt)

Composition parameters	Quartz	Calcite	Clay
K (GPa)	37.9	74.5	23.1
G (GPa)	44.3	30.6	11.7
ρ (g cc^{-1})	2.65	2.80	2.58

In the case of the hydrate in a fluid component model (Fig.4), the estimated P-wave velocity results are different from the measured P-wave velocity values, and the overall positions and trends of the two curves (velocity and density) are not as accurate as those of the original curves. This is particularly true in the hydrate-rich region at approximately 190–220 m below the seafloor. The P-wave velocity increases near the target formation under normal circumstances due to the velocity characteristics of the

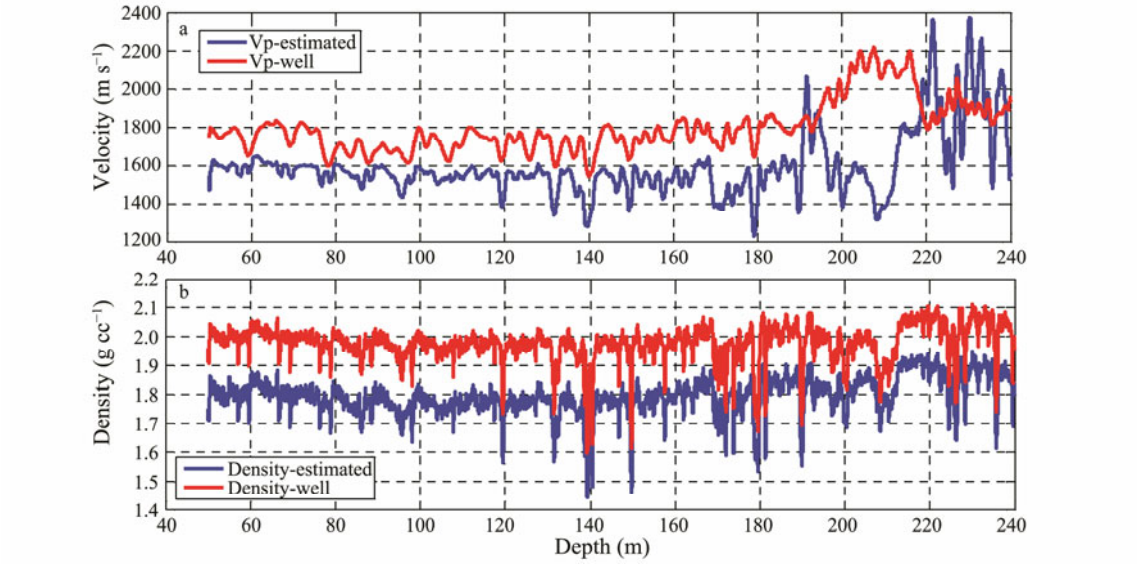

Fig.4 The P-wave velocity (a) and density (b) by multiple iterations of estimation results based on the fluid composition model of hydrates and known logging curves. a, shows the estimated P-wave velocity (blue) and the known P-wave velocity (red) of the well; b, depicts estimated density values (blue) and well-known density values (red).

hydrate. By contrast, compared to the local well curve (Fig.4), the P-wave velocity estimated locally decrease. Similarly, the estimated density values are quite different from those of the original logs. Because the volume fractions of calcite, quartz and other phases are modified by iterative calculations, as are the volume fractions of formation water and free gas presented in the fluid phase. The error of estimated P-wave velocity and the error of

the estimated density value can reach 72% and 43%, respectively. Thus, it can be inferred that the gas hydrate occurrence pattern in the Shenhu hydrate region is not likely the fluid phase. As a result, the fluid composition model for the hydrate phase cannot be used to estimate the S-wave velocity.

When the porosity ϕ is greater than the critical porosity ϕ_c:

$$K_{dry}=\left[\frac{(1-\phi)/(1-\phi_c)}{K_{HM}+\frac{4}{3}G_{HM}}+\frac{(\phi-\phi_c)/(1-\phi_c)}{\frac{4}{3}G_{HM}}\right]^{-1}-\frac{4}{3}G_{HM},$$

$$G_{dry}=\left[\frac{(1-\phi)/(1-\phi_c)}{G_{HM}+Z}+\frac{(\phi-\phi_c)/(1-\phi_c)}{Z}\right]^{-1}-Z,$$

$$Z=\frac{G_{HM}}{6}\left(\frac{9K_{HM}+8G_{HM}}{K_{HM}+2G_{HM}}\right). \quad (4)$$

In the first three hydrate cementation patterns, regardless of whether the hydrate is present at the contact site between rock particles, around the rock particles, or in the rock granule cementation, it acts as a constituent of the rock matrix, and it is part of the solid phase. Thus, it not only changes the original porosity of the formation but also affects the bulk modulus and shear modulus of the rock solid phase. Therefore, the relationship between the reduced porosity of the formation and the actual porosity of the formation is defined as:

$$\phi_r=\phi(1-S_h), \quad (5)$$

where S_h is he saturation of the hydrate in the rock pore. The volume modulus and the shear modulus of the rock skeleton of the hydrate layer are defined as:

$$K=\frac{1}{2}\left[f_hK_h+(1-f_h)K_s\right]+\frac{1}{2}\left[\frac{f_h}{K_h}+\frac{1-f_h}{K_s}\right]^{-1},$$

$$G=\frac{1}{2}\left[f_hG_h+(1-f_h)G_s\right]+\frac{1}{2}\left[\frac{f_h}{G_h}+\frac{1-f_h}{G_s}\right]^{-1}, \quad (6)$$

where K_S and G_S are the bulk modulus and the shear modulus of the solid phase of the rock skeleton, respectively, and f_h is the volume percentage of the hydrate within the solid skeleton. Additionally, the values of the bulk modulus and the shear modulus of the dry or saturated rock skeleton are the same as those used for the calculation of hydrate-free sediments.

This equation is estimated by the physical model of S-wave velocity:

$$V_P=[(K\_sat+4\cdot G\_sat/3)/\rho]\text{^}(1/2), \quad (7)$$

$$V_S=(G\_sat/\rho)\text{^}(1/2). \quad (8)$$

The final S-wave velocity estimated near the target layer (190–220 m) for the hydrate storage are shown in Fig.5. Similar to the P-wave velocity, the S-wave velocity increases. This estimation of the S-wave velocity also confirms the previous inference of the hydrate as a solid-phase model. The attenuation mechanism of S-wave velocity propagation is different from that of the P-wave velocity. In the physical model of S-wave estimation, the S-wave velocity is related to only the shear modulus parameter. P-wave can propagate through both solid and liquid phases, and their velocities are therefore affected by both solid and liquid phases. However, S-wave cannot propagate through the liquid phase, and thus, their velocities are affected by only the shear modulus, which is unrelated to those changes in the liquid phase.

Fig.5 shows the P-wave velocity, density and well-known curves obtained from repeated iterations based on a 'solid' hydrate composition model (Fig.6). The estimated P-wave velocity and density curves are in good agreement with the logging curve. The local minimum error of the density value is 0.3%, and the local minimum error of the P-wave velocity is 2.8%. The error indicates that the equivalent parameters of a rock mass cannot be estimated using the rock physical model due to its inability to account for the relationship between physical parameters, such as the shape of the rock skeleton, and other parameters, such as velocity and density. Between 60 and 180 m, the estimation results fit well with the basic changes in the original logging curve, but minor changes cannot be fully fit. Therefore, a relatively large error in the P-wave velocity still exists at depths of approximately 60–180 m. The volume percentage of the solid phase constituents of the rock (marble, quartz and hydrate) and the volume fraction of formation water and free gas in the rock pores were then modified (Table 3).

Table 3 Petrophysical parameters corresponding to final iteration estimates of S-wave velocity

Drilling number	Layer	Particle size composition (%)	
		Clay	Quartz + Calcite
SH2	Upper layer	26.71	73.29
	Hydrate layer	22.53	77.47
	Lower layer	23.55	76.45

The equivalent model takes into account the type of reservoir model for the hydrate (pore filling model), the occurrence form of hydrates (for the porosity greater than 40%, belonging to the cementitious state in the pore filling model), the interaction between phases and their interaction on the bulk modulus and shear modulus of the entire sediment layer. Therefore, the equivalent model is a relatively rigorous rock physics model, but it involves more parameters that are difficult to be determined, which also increases its uncertainty.

3.2 Estimation of S-Wave Velocity Based on the TPBE Model

The three-phase model was developed on the basis of the four-phase model. The four-phase Wood equations belong to the simple model. The equivalent medium theory (MBGL) is based on the first principle of physics. The simple model has simplified the factors affecting the

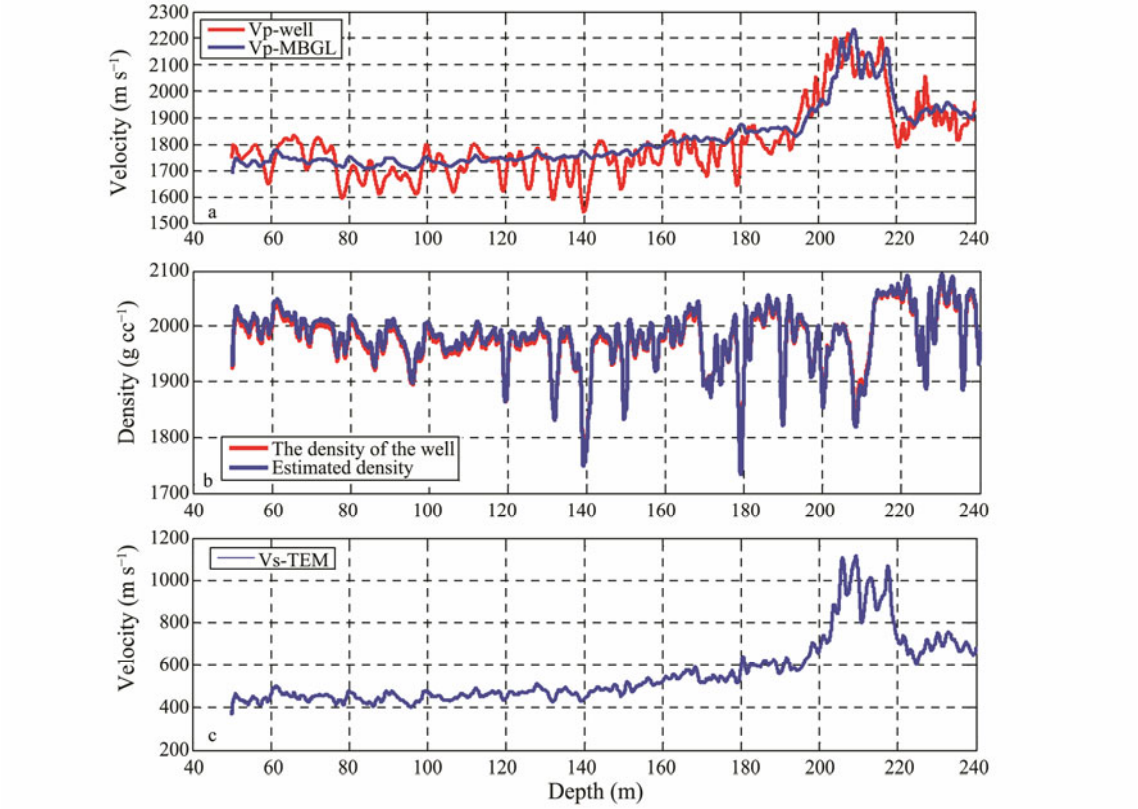

Fig.5 P-wave velocity and density based on multiple iterations for the hydrate as a solid component model and its comparison with the well-known curve. a, shows the estimated P-wave velocity (blue) with the well-known P-velocity (red); b, displays the estimated density (blue) and the well-known density (red); c, is the distribution of the estimated S-wave velocity.

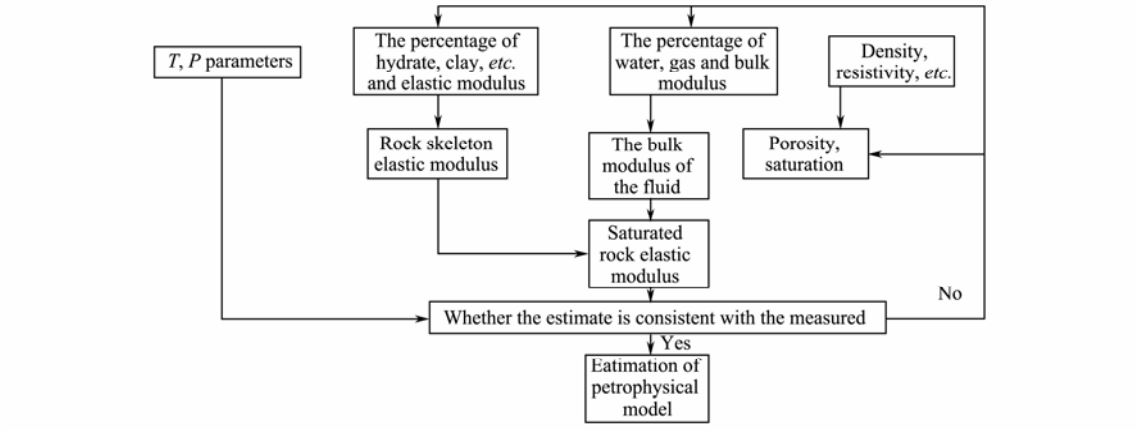

Fig.6 Flow chart of the S-wave velocity estimation in the solid-phase model.

hydrate saturation, and it lacks a rigorous theoretical basis. Although the equivalent medium method is strict, it involves many parameters. Additionally, the value is difficult to be determined, adding new uncertainties. Considering their respective advantages and disadvantages, based on the Wood equation of four-phase medium, hydrates are regarded as a part of the solid matrix. Equivalent medium theory is used to calculate the influence of hydrate on the rock matrix speed. The improved Wood equation is:

$$\frac{1}{\rho V_p^2}=\frac{\bar{\phi}S_w}{\rho_w V_w^2}+\frac{\bar{\phi}S_g}{\rho_g V_g^2}+\frac{1-\bar{\phi}}{\rho_m V_{mp}^2}, \tag{9}$$

where S_w and S_g are the saturation of water and free gas, with $S_w+S_g=1$; V_w, V_g, V_{mp} and V_p are the P-wave velocities of water, free gas, the rock matrix, and the hydrate deposition layer, respectively; and ρ_w, ρ_g, ρ_m, and ρ are the densities of water, free gas, the rock matrix, and the hydrate deposition layer, respectively. The presence of hydrates reduces the porosity, affects the velocity of the solid phase, so we recalculate the porosity, the mineral matrix fraction and density, the solid phase modulus K_m, G_m, then,

$$v_{mp}=\sqrt{(K_m+4G_m/3)/\rho_m}\ .$$

The density of the hydrate-bearing deposit is expressed as the weighted average of the individual component densities:

$$\rho = \varphi s_w \rho_w + \varphi s_g \rho_g + \varphi s_h \rho_h + (1-\varphi)\rho_m . \quad (10)$$

According to the empirical formula of the S-wave velocity estimation in the TPBE model in the hydrate occurrence area, the S-wave velocity is:

$$v_s = v_p[\alpha(1-\varphi) + \beta\varphi S + \gamma\varphi(1-S)], \quad (11)$$

$$\alpha = V_s/V_p \,|\,\text{matrix};\ \beta = V_s/V_{p\text{hydrate}};\ \gamma = V_s\,|\,V_{P\text{fluid}} .$$

The TPBE model considers the effect of the elastic modulus of each component in rock skeleton on the P- and S-wave velocities of the rock skeleton, but it does not consider the effect of the fluid phase in the pore medium. Therefore, the three-phase model is less accurate than the equivalent model.

Similarly, we continue to use the known P-wave velocity and density values as constraints to estimate the unknown shear-wave velocity in the TPBE model. According to the estimation results (Fig.7), the P-wave velocity estimated based on the TPBE model in the hydrate storage layer (190–220 m) has a range of 1900–2000 m s^{-1}, smaller than the actual P-wave velocity value in the range of 2100–2200 m s^{-1}. The density values are still well matched, and there is not much error in the proportion of rock composition. According to petrophysical theory, rock voids affect the elastic modulus of the entire rock skeleton. However, in the TPBE model, the solid, liquid and gas in the three-phase medium are independent of each other, and they are subject to their corresponding elastic modulus and shear modulus. In this way, the interaction between the media cannot be considered, and the model cannot match the rock structure characteristics observed in the Shenhu area. Thus, the estimation result is very different from that of the highly accurate MBGL model. The MBGL model considers all rock components as a whole to find the overall elastic modulus and the shear modulus and ultimately obtains the overall rock P-wave

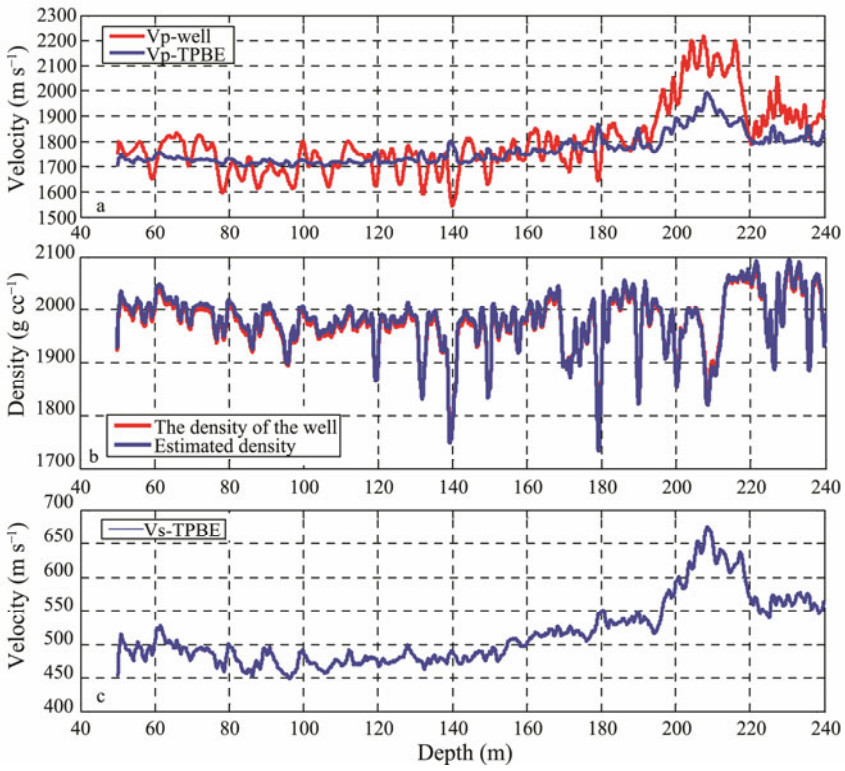

Fig.7 P-wave velocity and density estimated by multiple iterations based on the TPBE model when the hydrate is considered as a solid component and its comparison to the well-known curves. a, displays the estimated P-wave velocity (blue) with the well-known P-velocity (red); b, shows the estimated density (blue) and the well-known density (red); c, is the distribution of the estimated S-wave velocity.

velocity, taking into account the interaction between the various components of the rock. The model estimates the S-wave velocity to be in the range of 450–650 m s^{-1}, which is less than the estimated result based on the MBGL model.

3.3 Estimation of S-Wave Velocity Based on the TEM Model

The thermo-elasticity of rock refers to the compressive and expansion effect of the microscopic components of the rock when an elastic wave propagates through it during compression and expansion. The local temperature of the rock rises or falls so that the temperature difference occurs inside the rock and then generates heat transfer, causing the elastic wave attenuation of energy. The thermo-elastic properties of free gas and surrounding rock as well as natural gas hydrates are different (the free gas especially

has a higher thermal expansion coefficient, as shown in Table 4). Therefore, when the elastic wave passes through the surrounding rock and the hydrate reservoir, there will be different thermo-elastic responses. A greater hydrate saturation results in a greater difference.

Natural gas hydrates are generated at a certain temperature and pressure, and thus, hydrate reservoirs, especially those of gas, are more sensitive to temperature and pressure. Many previous studies of the P-wave velocity of the hydrate layer have used the TEM model (Wang *et al*., 2011), but no direct relationship between thermo-elastic parameters and S-wave velocity has been observed. It is difficult to obtain the direct relationship between the thermo-elasticity parameter and the S-wave velocity without rigorous physical experiments. Therefore, the direct relationship between the S-wave velocity and the P-wave velocity is obtained according to the empirical formula, then the indirect relationship between the S-wave velocity and the thermo-elasticity parameter is evaluated.

Table 4 Physical properties of various substances (Wang *et al*., 2006)

Type name	Density (kg m^{-3})	J (kg K)	10^{-5} K^{-1}
Rock	2650	750	0.11
Hydrate	767	2050–2200	1.04
Gas	88.48	2400	260
Oil	790–960	2200	22.89
Seawater	1095	4190	20.2

The P-wave velocity in the TEM model is calculated as follows:

$$v_p = \left\{ \left[\left(k + \frac{4}{3}\mu \right) + \frac{9k^2 a^2 T_0}{\rho_m c_e} \right] \right\}^{1/2}. \quad (12)$$

The effective thermal expansion coefficient α and the effective specific heat c_e are defined as:

$$\alpha = (1-\phi_{\text{eff}})\alpha_s + \phi_{\text{eff}}(S_w\alpha_w + S_g\alpha_g), \quad (13)$$

$$c_e = (1-\phi_{\text{eff}})c_{es} + \phi_{\text{eff}}(S_w c_{ew} + S_g c_{eg}). \quad (14)$$

According to the estimation results of the first two models, the density always has high stability precision, which shows that the rock component proportion error is negligible. From the point of view of the P-wave velocity, the results of the TEM model are in good agreement with the actual P-wave velocity values in the hydrate deposit horizon (190–220 m), with an error of approximately 3.6% (Fig.8). However, in the non-hydrate occurring horizon, the error is 51%, which is relatively large. The estimated S-wave velocity is in the range of 400–1100 m s^{-1} (according to empirical Eq. (9)), which is similar to the estimation result of the MBGL model. Therefore, the authors speculate that the TEM model is suitable for estimating the P-wave and S-wave velocities of the hydrate- bearing horizons due to the sensitivity of the properties of the gas

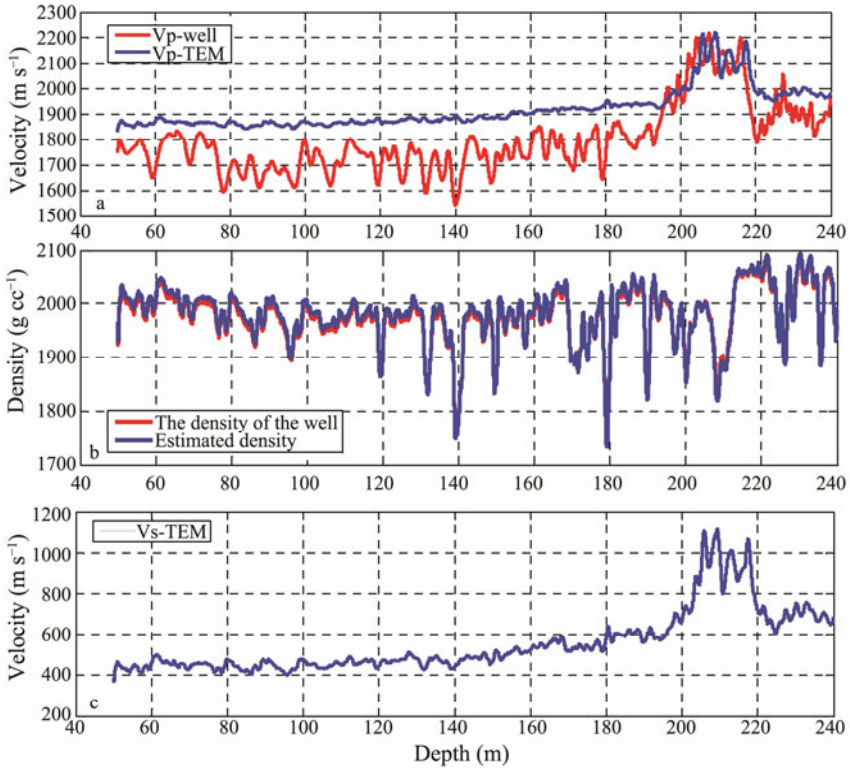

Fig.8 P-wave velocity and density estimated by multiple iterations based on the TEM model when the hydrate is considered as a solid component model and its comparison to the well-known curve. a, shows the estimated P-wave velocity (blue) with the well-known P-velocity (red); b, displays the estimated density (blue) and well-known density (red); c, is the distribution of the estimated S-wave velocity.

hydrate to temperature and pressure. However, in a formation where hydrates do not exist, the P-wave and S-wave velocity estimation accuracies are relatively low.

Fig.9a shows the results of the P-wave velocity estimation based on three models and the acoustic velocity log. Fig.9b shows the results of the S-wave velocity estimation of the three models. The estimation results for the P-wave based on the MBGL model and the TEM model are in good agreement with the logging acoustic curve in the hydrate bearing layers (190–220 m), with errors of 2.8% and 3.6%, respectively. The estimation accuracy of the TPBE model is low, and the error reached 46.6%. The estimation results of the P-wave velocity based on the MBGL model and the TPBE model are in good agreement with the logging acoustic curve for the layers without the hydrate, with errors of 3.1% and 5.5%, respectively, but the estimated error of the TEM model is 51.3%. Therefore, for the hydrate bearing layers, the appropriate P-wave and S-wave velocity estimation models are both the MBGL model and the TEM model.

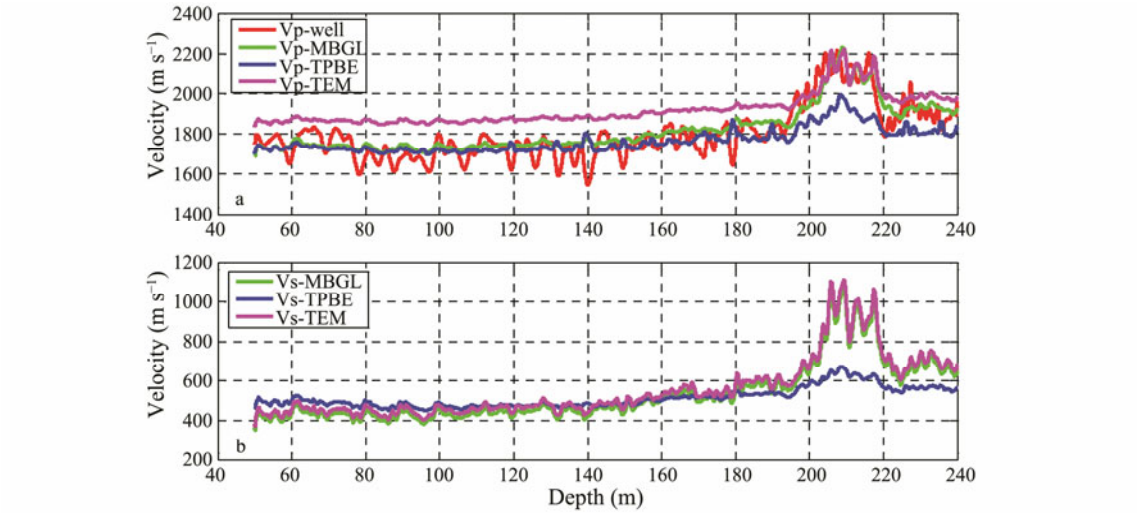

Fig.9 Comparison of the P-wave (a) and S-wave velocities (b) based on the three models.

The S-wave velocity estimation results for the MBGL model and the TEM model are very similar (Fig.9b), and the reciprocal relationship between the P-wave velocity and the S-wave velocity is approximately two. However, the results of the TPBE model are quite different. If the P-wave velocity and density are used as the constraint criteria to determine the accuracy of the S-wave velocity estimation results, the MBGL model is the most suitable physical model for the Shenhu area, followed by the TEM model; the worst model is the TPBE model.

3.4 Application

The seismic data used in this paper are from horizontal cable SH000 (2D), as shown in the right portion of Fig.1. The air gun used in this study had a source capacity of 540 inch^3, a working pressure of 2000 psi, a run spacing of 25 m, a depth of 5 m, and a main frequency of 100 Hz. The data were preprocessed, and the P-wave velocity, the S-wave velocity, Poisson's ratio, and other variables were inverted using the pre-stack AVO inversion method according to logging and seismic data from the study area (Figs.10–13).

In the non-perpendicular incident state, the elastic wave generated by the source on the ground propagates downwards. When it reaches the stratigraphic interface, the reflected P-wave, the reflected S-wave, the transmitted P-wave and the transmitted S-wave are generated. In a homogeneous medium, the Zoeppritz equation of the downstream P-wave can be obtained according to the continuity principle of the displacement stress in the normal direction and the tangential direction. With the continuous development of the theory, many approximate formulae have been derived. In this paper, the Shuey approximation formula is used (Shuey, 1985). The elastic modulus and the shear modulus of the rock are used to replace the P-wave velocity and the shear-wave velocity in the equation. The equations of the petrophysical parameters can be expressed as follows.

$$R(\theta)\approx A+B\sin^2\theta+C(\tan^2\theta-\sin^2\theta)\,, \tag{15}$$

$$A=\frac{1}{2}\left(\frac{\Delta v_p}{v_p}+\frac{\Delta\rho}{\rho}\right), \tag{16}$$

$$B=\frac{1}{2}\frac{\Delta v_p}{v_p}-4\frac{v_s^2}{v_p^2}\frac{\Delta v_s}{v_s}-\frac{v_s^2}{v_p^2}\frac{\Delta\rho}{\rho}, \tag{17}$$

$$C=\frac{1}{2}\frac{\Delta v_p}{v_p}. \tag{18}$$

Pre-stack elastic inversion is performed on the seismic data alongside the logging data (Fig.11) with the estimated S-wave velocity data using the petrophysical method. According to the obtained P-wave velocity section (Fig.11), the inversion results for the hydrate reservoirs are in good agreement with the P-wave velocity anomalies. According to the obtained S-wave velocity section (Fig.12), the hydrate reservoirs correspond to the S-wave velocity anomalies, but their visibility to the hydrate layer is less

than that of the P-wave velocity. Therefore, according to the Poisson's ratio profile (Fig.13), the hydrate reservoir has a very clear interface with the surrounding rock. The Poisson's ratio of the reservoir is smaller than those of the upper and lower rocks, whereas the Poisson's ratio of the upper rock of the hydrate is slightly larger than that of the lower rock. It can be inferred that the lower rock of hydrate may be rich in free gas.

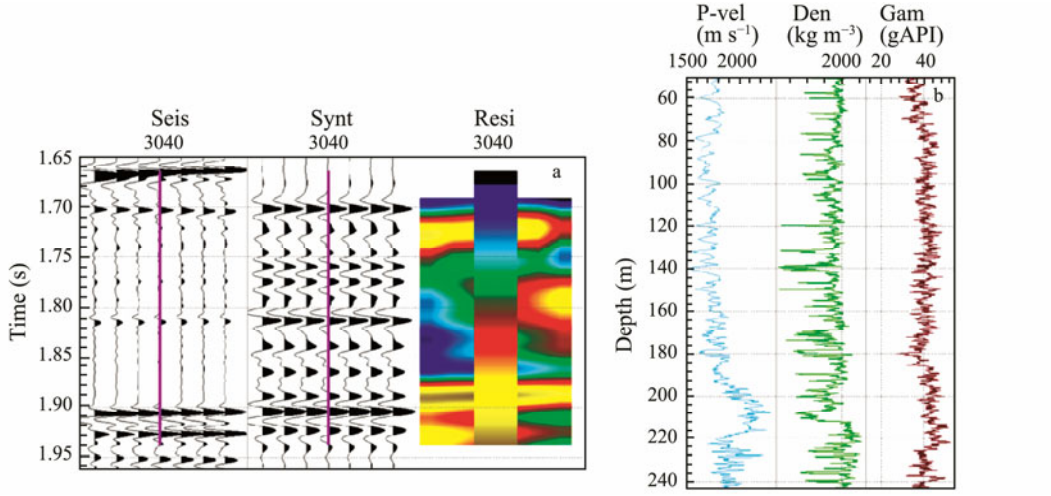

Fig.10 Results of well-seismic calibration. a, the left image is the raw data; the middle image is the synthetic seismic record; and the right image is their correlations); b, the logs of well SH2. The light blue line is the P-velocity log; the grass green line is the density log; and the gray line on the right is the Gamma log.

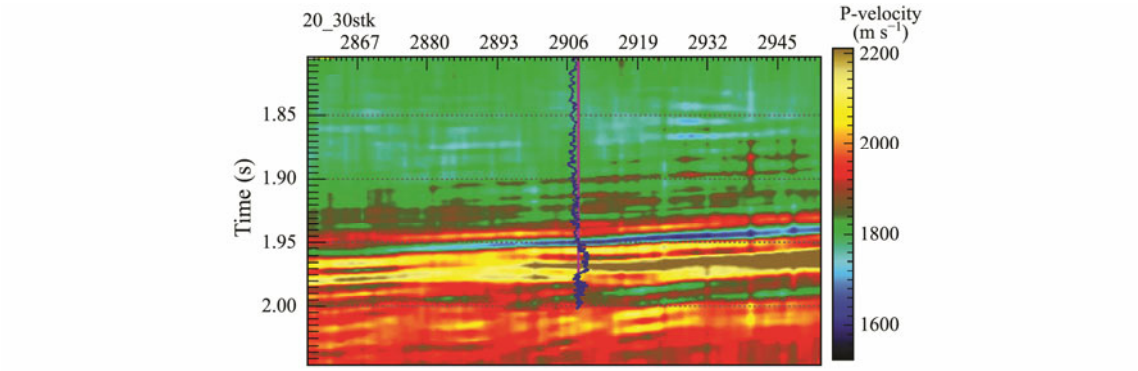

Fig.11 P-wave velocity distribution obtained by elastic inversion.

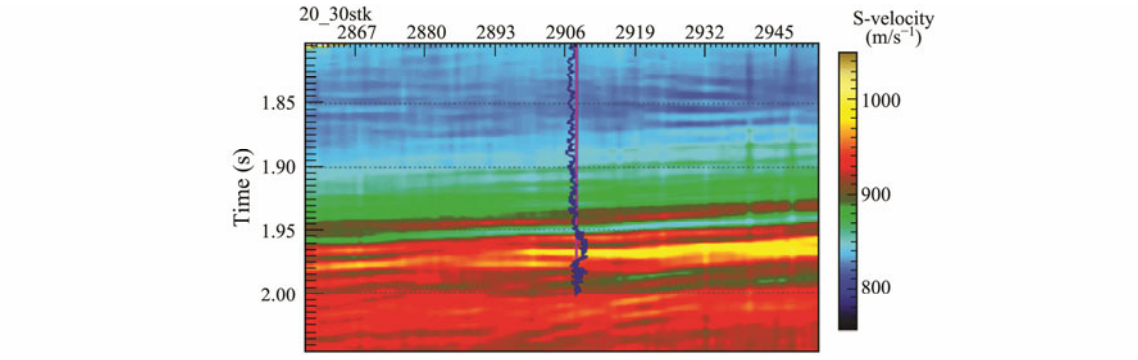

Fig.12 S-wave velocity distribution obtained by elastic inversion.

4 Conclusions

1) In this paper, logging data from the Shenhu area in the northern South China Sea and the rock physical parameters obtained from previous studies were analyzed and summarized. Based on the results of the porosity analysis, a suitable method for the formation with the porosity greater than 40% was modified according to the critical porosity theory of Nur (Nur *et al*., 2000).

2) Two hydrate occurrence state models, based on the Gassmann hydrate rock physical model, are discussed in

this paper (occurrence model one, the hydrate is the liquid phase; occurrence model two, the hydrate is the solid phase). Based on the estimates of these two models, the model that considers the hydrate as a fluid phase is discarded because its results contrast with the known data. Model 2 that considers the hydrate as a solid-phase is selected because its estimated results are in good agreement with the known conditions.

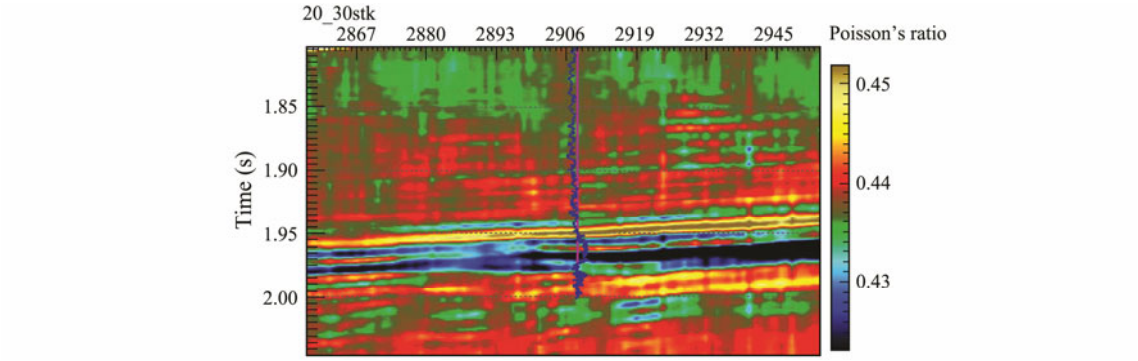

Fig.13 Poisson's ratio distribution obtained by elastic inversion.

3) The first criterion of the MBGL is based on the physical properties. The MBGL model considers the intrinsic relationship between the various rock components. In this model, there is a more rigorous theoretical relationship between the petrophysical parameters and the P-wave and S-wave velocities. By using this model, reasonable S-wave velocities (values ranging from 400–1100 $m\,s^{-1}$ and for hydrate layers of 1100 $m\,s^{-1}$) were obtained for the Shenhu area. The TEM model particularly reflected the temperature and pressure sensitivity of gas hydrates. In the velocity estimation model of TEM, there are thermo-elastic parameters as well as petrophysical parameters. Therefore, the model also takes into account the petrophysical properties and thermo-elastic properties. The MBGL model and the TEM model have good applicability for estimating the P-wave and S-wave velocities of hydrate-bearing layers. The TPBE model is a partial simplification of the MBGL model, which is more applicable under some conditions. However, the accuracy of the TPBE is far worse than that of the MBGL when rock physics parameters are relatively accurate.

Acknowledgements

The study is supported by the National Natural Science Foundation of China (Nos. 41304096 and 41176077), the National Science and Technology Major Project of China (No. 2016ZX05024-001-002), the National High-tech R&D Program of China (863 Program; No. 2013AA0925 01), and the Fundamental Research Funds for the Central Universities (No. 201762019).

References

Castagna, J. P., Batzle, M. L., and Eastwood, R. L., 1985. Relationship between compressional wave and shearwave velocities in clastic silicate rock. *Geophysics*, **50** (4): 571-581.

Castagna, J. P., Batzle, M. L., and Kan, T. K., 1993. Rock physics – The link between rock properties and AVO response. In: *Offset-Dependent Reflectivity – Theory and Practice of AVO Analysis, Investigations in Geophysics, Society of Exploration Geophysisicists*. Tulsa, USA, 135-171.

Chen, F., Su, X., Zhou, Y., Lu, H, F., and Liu, G., 2009. Variations in biogenic components of late Miocene Holocene sediments from Shenhu area in the northern South China Sea and their geological implication. *Marine Geology & Quaternary Geology*, **29**: 1-8.

Chen, F., Zhou, Y., Su, X., Liu, G., and Lu, G., 2011. Gas hydrate saturation and its relation with grain size of the hydrate-bearing sediments in the Shenhu area of northern South China Sea. *Marine Geology & Quaternary Geology*, **31** (5): 95-100.

Cheng, W, B., Wu, Y, R., Liang, C. W., Lin, J, Y., and Hsu, S. K., 2018. Imaging P- and S-wave velocity structures in hydrate bearing sediments along an OBS profile across the Yuan-An Ridge, off southwest Taiwan. *Terrestrial Atmospheric & Oceanic Sciences*, **29** (1): 39-50.

Dai, J., Xu, H, B., Snyder, F., and Dutta, N., 2004. Detection and estimation of gas hydrates using rock physics and seismic inversion: Examples from the northern deepwater Gulf of Mexico. *The Leading Edge*, **23** (1): 60-66.

Dong, N., Huo, Z. Z., Sun, Z. D., Liu, Z. S., and Sun, Y. Y., 2014. An investigation of a new rock physics model for shale. *Journal of Geophysics*, **57** (6): 1990-1998 (in Chinese with English abstract).

Ecker, C., Dvorkin, J., and Nur, A., 1998. Sediments within gas hydrates: Internal structure from seismic AVO. *Geophysics*, **63** (5): 1659-1669.

Fu, S. Y., and Lu, J. A., 2010. The characteristics and origin of gas hydrate in Shenhu area, South China Sea. *Ocean Geology Dynamics*, **26** (9): 6-10 (in Chinese with English abstract).

Krief, M., Garat, J., Stellingwerff, J., and Ventre, J., 1990. A petrophysical interpretation using the velocities of P and S waves (full-waveform sonic). *The Log Analyst*, **31**: 355-369.

Lin, H. W., 2015. A method for S-wave velocity estimation based on rock physical analysis. Master thesis. Chengdu University of Technology.

Li, Q. Z., 1992. Characteristics of P-wave and S-wave velocity of rock. *Petroleum Geophysical Prospecting*, **27** (1): 1-12 (in Chinese with English abstract).

Ma, Y., Kong, L., Liang, Q. Y., Lin, J. Q., and Li, S. Z., 2014. Characteristics of hazardous geology factors on the Shenhu continental slope in the northern South China Sea. *Earth Science–Journal of China University of Geosciences*, **36** (9): 1364-1372 (in Chinese with English abstract).

Mavko, G., Mukerji, T., and Dvorkin, J., 2009. *The Rock Physics Handbook: Tools for Seismic Analysis in Porous Media*. Cambridge University Press, Cambridge, U. K., 1-503.

Mindlin, R. D., 1949. Compliance of elastic bodies in contact. *Journal of Applied Mechanics*, **16** (3): 259-268.

Milholland, P., Manghnani, M. H., Schlanger, S. O., and Sutton, G. H., 1980. Geoacoustic modeling of deep-sea carbonate sediments. *Journal of the Acoustical Society of America*, **68** (5): 1351-1360.

Nur, A., Mavko, G., Dvorkin, J., and Galmudi, D., 2000. Critical porosity: A key to relating physical properties to porosity on rocks. *Leading Edge*, **17** (1): 878-881.

Shuey, R. T., 1985. A simplification of the Zoeppritz equations. *Geophysics*, **50**: 609-614.

Wang, X., Hutchinson, D. R., Wu, S., Yang, S., and Guo, Y., 2011. Elevated gas hydrate saturation within silt and silty clay sediments in the Shenhu area, South China Sea. *Journal of Geophysical Research: Solid Earth*, **116** (B5): 35-52.

Wang, X. J., Wu, S. G., and Liu, X. W., 2006. Factors affecting the estimation of gas hydrate and free gas saturation. *Chinese Journal of Geophysics*, **49** (2): 504-511 (in Chinese with English abstract).

Wu, N. Y., Yang, S, X., and Wang, H. B., 2009. Gas-bearing fluid influx sub-system for gas hydrate geological system in Shenhu area, northern South China Sea. *Chinese Journal of Geophysics*, **52** (6): 1641-1650.

Wu, N. Y., Zhang, H. Q., Yang, S. X., Liang, J. Q., and Wang, H. B., 2007. Preliminary discussion on natural gas hydrate (NGH) reservoir system Shenhu area, north slope of South China Sea. *Natural Gas Industry*, **57** (5): 1664-1674 (in Chinese with English abstract).

Wu, S. G., Xie, Y. B., Qin, Q., and Li, Q. P., 2014. Shallow drilling geological disasters of oil and gas in deepwater. *Prospecting Engineering*, **24** (9): 38-42 (in Chinese with English abstract).

Xing, L., Liu, X. Q., Zhang, J., Liu, H. S., Zhang, J., Li, Z. Z., and Wang, J. H., 2018. Sensitivity analysis of P-waves and S-waves to gas hydrate in the Shenhu area using OBS. *Journal of Ocean University of China*, **17** (1): 139-146.

Xu, S., and White, R. E., 1995. A new velocity model for sand-clay mixtures. *Geophysical Prospecting*, **43** (1): 91-118.

Zhang, G. Z., Chen, H. Z., Wang, Q., and Yin, X. Y., 2013. Estimation of S-wave velocity and anisotropic parameters using fractured carbonate rock physics model. *Journal of Geophysics*, **56** (5): 1707-1715 (in Chinese with English abstract).

Zhang, X. G., Xu, H. N., Liu, X. W., Zhang, M., Wu, Z. L., Liang, J. Q., Wang, H. B., and Sha, Z. B., 2014. The acoustic velocity characteristics of sediment with gas hydrate revealed by integrated exploration of 3D seismic and OBS data in Shenhu area. *Journal of Geophysics*, **57** (4): 1169-1176.

(Edited by Chen Wenwen)